Biosensors and Bioelectronics 133 (2019) 183–191

Contents lists available at ScienceDirect

Biosensors and Bioelectronics

journal homepage: www.elsevier.com/locate/bios

Multi-site dynamic recording for Aβ oligomers-induced Alzheimer's disease *in vitro* based on neuronal network chip

Fan Gao[1], Keqiang Gao[1], Chuanjiang He, Mengxue Liu, Hao Wan*, Ping Wang*

Biosensor National Special Laboratory, Key Laboratory for Biomedical Engineering of Education Ministry, Department of Biomedical Engineering, Zhejiang University, Hangzhou, Zhejiang 310027, China

ARTICLE INFO

Keywords:
Neuronal network chip
Alzheimer's disease
Amyloid-β oligomers
Microelectrode array
Electrical stimulation

ABSTRACT

Alzheimer's disease (AD) is a chronic central neurodegenerative disease. The pathological features of AD are the extracellular deposition of senile plaques formed by amyloid-β oligomers (AβOs) and the intracellular accumulation of neurofibrillary tangles. However, due to the lack of effective method and experimental models to study the cognitive decline, communication at cell resolution and the implementation of interventions, the diagnosis and treatment on AD still progress slowly. In this paper, we established a pathological model of AD *in vitro* based on AβOs-induced hippocampal neuronal network chip for multi-site dynamic analysis of the neuronal electrical activity and network connection. The multiple characteristic parameters, including positive and negative spike intervals, firing rate and peak-to-peak values, were extracted through the analysis of spike signals, and two firing patterns from the interneurons and pyramidal neurons were recorded. The spatial firing patterns mapping and cross-correlation between channels were performed to validate the degeneration of neuronal network connectivity. Moreover, an electrical stimulation with frequency at 40 Hz was exerted to preliminarily explore the therapeutic effect on the pathological model of AD. This neuronal network chip enables the implementation of AD models *in vitro* for studying basic mechanisms of neurodegeneration within networks and for the parallel testing of various potential therapies. It can be a novel technique in the research of AD pathological model *in vitro*.

1. Introduction

Alzheimer's disease (AD) is a chronic central neurodegenerative disease which is characterized by comprehensive dementia such as short-term memory disorder and cognitive impairment. Meanwhile, it will cause the atrophy of the cerebral and severe shrinkage of hippocampus. In the current society, aging of the population has increased significantly, whereas the diagnostic tools are limited. Thus, the high incidence and disability rate of AD has become a major issue affecting human health. As shown in Fig. 1, the previous researches have indicated that the pathological features of AD are the extracellular deposition of senile plaques formed by amyloid-β oligomers (AβOs) and the intracellular accumulation of neurofibrillary tangles (NFTs) formed by hyperphosphorylated tau protein (Hyman et al., 2012). Aβ peptides are comprised of 39–43 amino acids which are generated from amyloid precursor protein (Sosa et al., 2017). The synaptic dysfunction and cognitive reduction were closely related to the synaptotoxicity of AβOs, which are the major form of Aβ aggregates (Sheng et al., 2012). AβOs have opened axonal voltage-gated calcium channels that facilitate calcium influx, eventually leading to the injury of axonal transport of cargos, such as brain-derived neurotrophic factor (Gan and Silverman, 2015). NMDA receptors are the key type of ionotropic glutamate receptors on excitatory postsynaptic membranes (Scheefhals and MacGillavry, 2018). AβOs co-located with NMDA receptor-containing protein complexes at the neuronal surface could elicit distinct downstream pathways to induce the synaptotoxic effects (Decker et al., 2010). Tau is a microtubule-associated protein binding the microtubule in neurons, which predominantly enrich in axons. Tau can stabilize the microtubule and undergo different kinds of posttranslational modifications, such as phosphorylation, glycosylation, acetylation, ubiquitination, *etc.* Aberrant modifications, such as the abnormal hyperphosphorylation, can induce conformational changes and aggregation of tau that results in the formation of NFTs (Morris et al., 2011). In the neuronal network of the AD model, the pathological hyperphosphorylation of tau has been detached from microtubules because of its structural changes. Meanwhile, the stability of cytoskeleton has

* Corresponding authors.
E-mail addresses: wh1816@zju.edu.cn (H. Wan), cnpwang@zju.edu.cn (P. Wang).
[1] Contribute equally to this work.

https://doi.org/10.1016/j.bios.2019.03.025
Received 18 January 2019; Received in revised form 11 March 2019; Accepted 13 March 2019
Available online 14 March 2019
0956-5663/

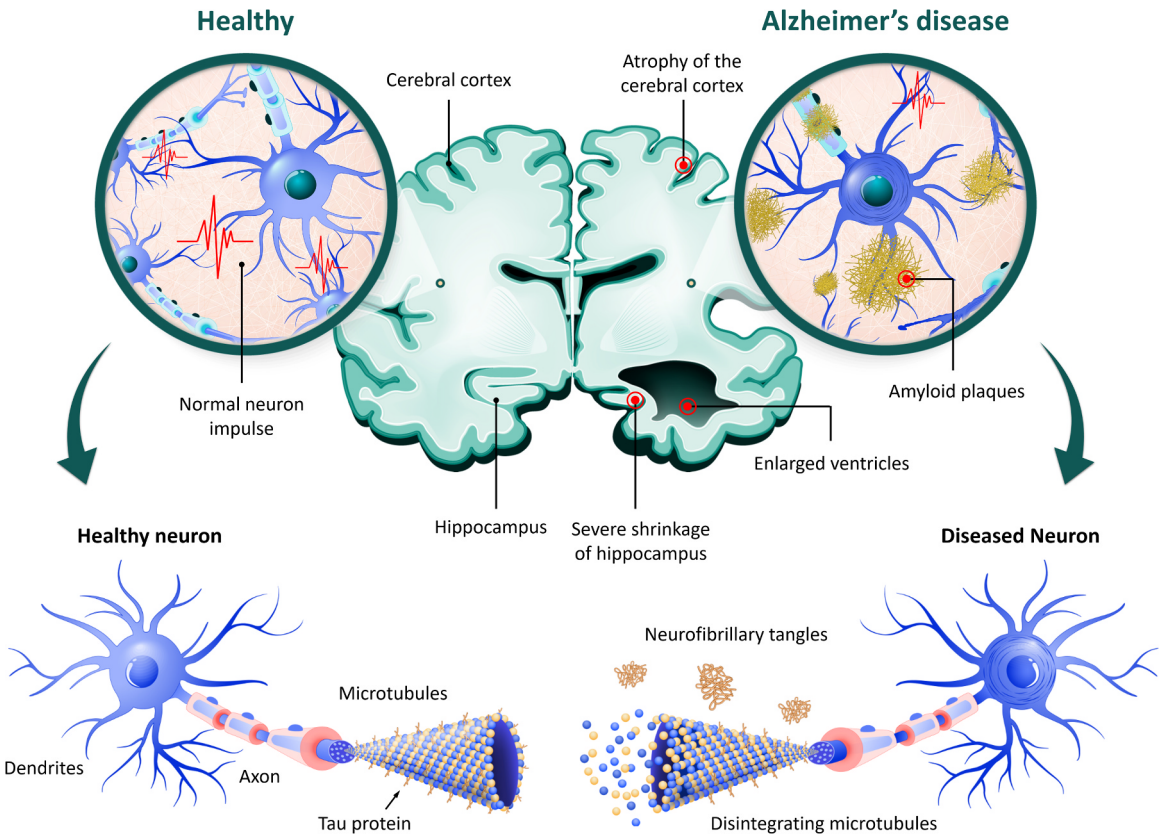

Fig. 1. The pathological features of AD, mainly including the atrophy of the cerebral and severe shrinkage of hippocampus, the extracellular deposition of senile plaques formed by AβOs and the intracellular accumulation of neurofibrillary tangles formed by hyperphosphorylated tau protein.

decreased (Kanaan et al., 2012; Stern et al., 2017). In addition, pathological tau can bind to synaptic vesicles by its N-terminal sequence eventually causing the disruption of presynaptic functions (Mcinnes et al., 2018).

In recent years, some researchers have established the pathological model of AD through neurons or organotypic brain slices exposed to AβOs *in vitro* (Bomfim et al., 2012; Tu et al., 2014). Various techniques such as patch clamp and functional optical imaging have been applied to study ion channels and neuronal electrical activities. The patch clamp is a gold standard recording method with high sensitivity and specificity. However, it is difficult to reveal the neuron network characteristics due to its limited number of channels and complicated operations required (April et al., 2015; Cai et al., 2013; Lu and Gean, 1998). Calcium ion imaging can perform multiple single-cell activity mapping but is typically limited by the low temporal resolution and the difficulty in conducting continuous on-line recordings for a long time (Andermann et al., 2010). Microelectrode array (MEA) can record the extracellular membrane action potential generated by transport of transmembrane ion with the advantages of high readouts, noninvasiveness, long-term simultaneous recording and stimulation (Charkhkar et al., 2015). Hence, it has become a promising measurement platform for electrophysiological studies of neuronal networks (Cottance et al., 2013). Many reports used MEA (Keefer et al., 2001; Novellino et al., 2011; Robinette et al., 2011; Stett et al., 2003) or complementary metal-oxide semiconductor-multi-electrode arrays (CMOS-MEA) (Alessandro et al., 2010; Berdondini et al., 2001; Eversmann et al., 2003; Franks et al., 2003) to study the activity of neuronal networks. A CMOS-MEAs system was used to characterize the early activity-dependent changes induced by AβOs in neuronal networks for neurotoxicity (Amin et al., 2017). However, they did not specifically classify neurons, so it was hard to observe the different effects by AβOs on the interneurons and pyramidal neurons, and no electrical stimulation was given as intervention. To overcome these limitations, we established a pathological model of AD *in vitro* based on AβOs-induced hippocampal neuronal network chip for multi-site dynamic analysis of the neuronal electrical activity and network connection. The spatial firing patterns mapping and cross-correlation between channels were performed to validate the degeneration of neuronal network connectivity. Moreover, an electrical stimulation with frequency at 40 Hz was exerted to preliminarily explore the therapeutic effect on the pathological model of AD.

2. Material and methods

2.1. MEA chip and recording system

The MEA chip consists of multi-channels to record the signal from the electroactive neural network. After the neurons grow on the chip surface, spontaneous or excitatory stimulation produces a large amount of transmembrane ion transport to generate action potential and changes the extracellular membrane potential. MEA chips were fabricated by the technology of MEMS and its general process is shown in Fig. S1A. The MEA was electroplated with platinum black by chronoamperometry to increase the specific surface area and reduce the impedance of the electrodes and to improve the signal to noise ratio (SNR). AC impedance spectroscopy was used to evaluate the electrodes surface characteristics. The impedance amplitude of bare gold electrode decreased rapidly with the increase of frequency, while platinum black plating significantly reduced the impedance (Fig. S1B).

The detailed working principle diagram of the MEA chip is shown in Fig. S2. R_{mi} is metal interconnect resistance and Z_e is double layer impedance at the electrode-electrolyte interface. The voltage at the electrode-electrolyte interface is close to the voltage near the cell membrane. The change of cell membrane potential directly affects the

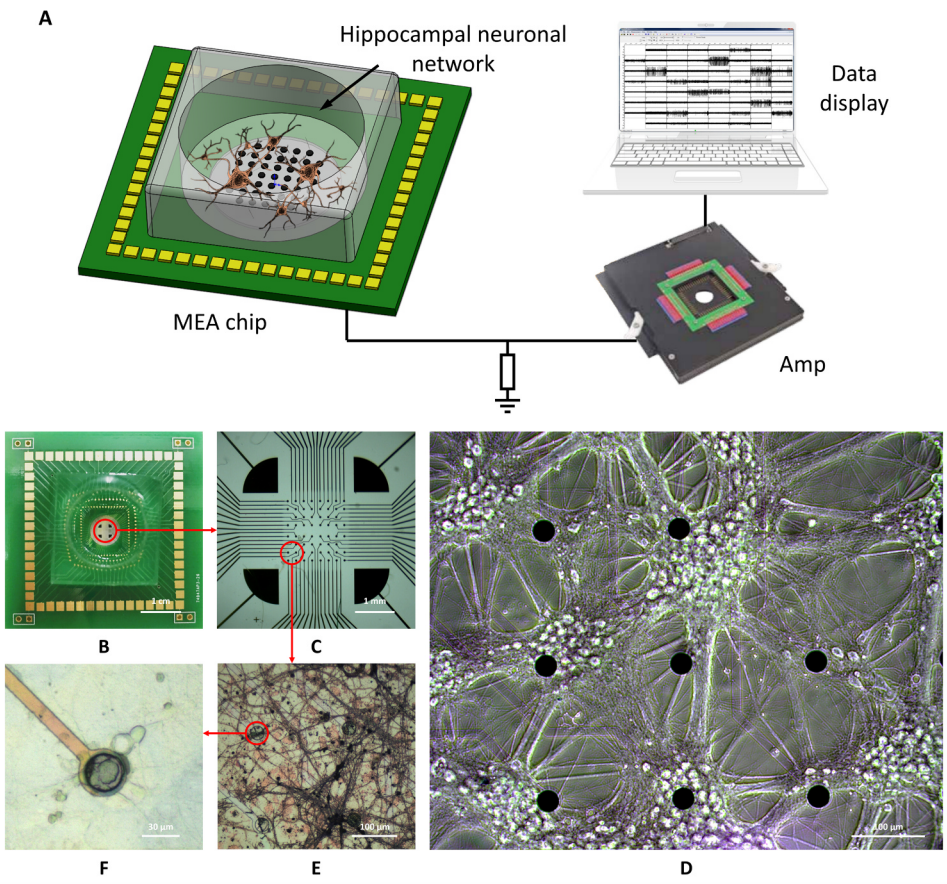

Fig. 2. MEA chip and hippocampal neuronal network. (a) The schematic diagram of the MEA system mode. (b) The assembled MEA chip with PDMS cavity. (c) The MEA chip electrodes arrays. (d) The growth of hippocampal neuronal network on the chip surface under microscope and (e) after Wright's dye staining. (f) The soma and axon dendrites of neurons growing on the electrode surface.

voltage at this point. The schematic diagram of the MEA system mode is shown in Fig. 2A. Multi-electrode channels were wired out and connected to external modules that are designed for neural signal amplification, filtering, data processing, and analysis. The signal was recorded by the electrode point followed by the amplifier, then was transmitted to the PC for display and analysis by the data acquisition card. The temperature of the MEA chip was controlled at 37 °C via a temperature control module. Stimulation sequence with different amplitudes and frequencies can be programmed and exerted to any electrode point via a stimulation module, and the post-stimulation responses of all channels can be recorded synchronously.

2.2. Preparation of the $A\beta_{1-42}$ oligomers

$A\beta_{1-42}$ oligomers were prepared from synthetic as previously described (De Felice et al., 2007; Geng et al., 2013; Lambert et al., 1998). Firstly, peptide vial was opened which allowed lyophilized $A\beta_{1-42}$ (Invitrogen) to equilibrate for 30 min at room temperature. Secondly, $A\beta_{1-42}$ peptide was re-suspended in the cold 1,1,1,3,3,3-hexafluoro-2-propanol (HFLP) (Sigma) and vortexed in the solution for a few seconds. Then, we quickly divided the $A\beta_{1-42}$/HFLP solution equally into three polypropylene vials. Thirdly, the vials were incubated for 2 h at room temperature to allow for Aβ monomerization. Then, we concentrated the solution under a vacuum by using a SpeedVac centrifuge (800 G, room temperature) until a clear peptide film was observed at the bottom of the vials. Finally, the peptide film was re-suspended by adding dimethylsulfoxide (DMSO) to obtain a concentration of up to 5 mM, and the vials were sealed and stored at −20 °C. Before the experiment, we diluted the obtained 5 mM $A\beta_{1-42}$/DMSO aliquot with 100 μL 0.01 M sterile phosphate buffer (PBS), then vortexed it for 30 s and incubated it for 12 h at 4 °C. For treatment of cells, we added the solution into the neurobasal medium to make sure that the final concentration was 500 nM.

2.3. Hippocampal neuron culture

All experiments involving animals were carried out in accordance with the ethical guidelines of the Zhejiang University Animal Experimentation Committee. The pregnant Sprague-Dawley (SD) rat was obtained from Zhejiang Academy of Medical Sciences. The operational steps were as follows (Hu et al., 2015; Tang et al., 2015; Yang et al., 2016). MEA chips were coated with poly-D-lysine and laminin (Sigma) mixture at 4 °C overnight in advance to improve the biocompatibility. Hippocampal tissues were harvested from the fetuses and chopped gently and digested in 0.25% trypsin (Gibco) for 15 min at 37 °C. The dissociated cells were plated at a density of $1 * 10^4/cm^2$ for immunocytochemistry on 24-well plate and $5 * 10^5$/well on the surface of the MEA chip in the plating medium (DMEM containing 10% Horse Serum) (Gibco) and maintained in an incubator at 37 °C under 5% CO_2. After plating for 4 h, the plating medium was substituted by neurobasal medium (neurobasal containing 2% B27 supplement, 1% glutamax and 0.4% Penicillin-Streptomycin) (Gibco). At plating DIV 3, cytosine arabinofuranoside with a final concentration of 2.5 μM was added, and the medium was half replaced every 2–3 d. The neurons were induced by $A\beta_{1-42}$ at DIV 13, and then the neurons on MEA chips were used for electrophysiological recording at different time points. After being induced for 12 h, the neurons at 24-well plate were used for immunofluorescence staining.

2.4. Immunofluorescence staining

In this experiment, the neurons were fixed with 4% paraformaldehyde at room temperature for 30 min. They were washed by PBS buffer

for three times and permeabilized with 0.15% Triton X-100 for 15 min. Then, they were incubated with a blocking solution of 1% BSA for 30 min at 37 °C. After that, the neurons were incubated with a primary antibody (MAP2, p-tau) at 4 °C for 12 h and were incubated with Alexa Fluor secondary antibody at room temperature for 2 h. The nuclei of the cells were finally stained by the DAPI staining and mounted on glass slides. The primary antibodies were diluted by a solution containing 1% Triton X-100, 5% goat serum and 1% BSA with a dilution ratio of 1:250 (MAP2) (Proteintech) and 1:200 (p-tau) (Cell Signaling Technology) respectively. The Alexa Fluor secondary antibody (Beyotime) was diluted by a PBS solution with a dilution ratio of 1:500. The images were captured by Laser confocal fluorescence microscopy (Nikon).

2.5. Statistical analysis

The MEA data were recorded and replayed in MC_Rack (Multi Channel Systems, Germany). The waveforms of spontaneous action potentials were sorted out after the raw signals were filtered by a high-pass filter with a cutoff frequency at 250 Hz. The signals of all channels were analyzed by calculating positive and negative spike intervals, firing rates and peak-to-peak values. All data in this work were expressed as the mean ± standard error of the mean (SEM). Differences between groups were examined for statistical significance, which was assessed by the Student's *t*-test. To ensure the consistency and reproducibility of our results, we conducted at least three repeated trials performing in different culture preparations and from at least three different animals. The number of samples used in each experiment is depicted in the figure legends.

3. Results and discussion

3.1. Hippocampal neuron cultured on MEA chip

The assembled MEA chip is shown in Fig. 2B. The cavity with a diameter of 1.5 cm and height of 1 cm was fabricated by PDMS and fixed on the chip for cell culture. The bonding pads on the MEA chip and the interfaces on PCB were connected by gold thread. The MEA chip consists of 60 working electrodes arranged in 8 × 8 square arrays. The diameter of single electrode is 30 μM and the interelectrode distance (center to center) is 200 μm (Fig. 2C). The growth of hippocampal neuronal network on the chip surface under microscope is shown in Fig. 2D and Fig. 2E (after Wright's dye staining). It indicates that the MEA chip surface has good biocompatibility and the neuronal network has been well formed. As shown in Fig. 2F, the soma and axon dendrites of neurons were visibly attached to one single electrode, leading to the assembly of signals from several neurons recorded by one electrode. The firing of neurons attached to the electrodes is the basis for MEA detection (Hu et al., 2015).

3.2. Immunofluorescence imaging analysis

To verify the effect of neurons treated with AβOs, we used Microtubule Associated Protein (MAP2), which is another member of the microtubule-associated protein family that is exclusively localized to dendrites to observe the changes in cell morphology (Li and Götz, 2017). Immunofluorescence staining for MAP2 revealed the neurites degeneration and dendrites impairment after treatment with AβOs for 12 h (Fig. 3A). Moreover, the staining with p-tau antibody was performed and the p-tau levels were strongly increased in a small portion of AβOs-induced neurons (Fig. 3B). The mean fluorescence intensity was also used to quantify the p-tau levels and the great significant difference between the control and AβOs-treated group are shown in Fig. 3C. In Alzheimer's disease, tau protein is hyperphosphorylated and abnormally accumulates in axons, dendrites and cell bodies (Se Hoon et al., 2011). Our results validated that the p-tau proteins were aggregated similarly to those observed in the degenerating neurons of AD in the previously mentioned reports.

3.3. Neuron firing patterns analysis

When the hippocampal neuronal network had grown for 13 days on the MEA chip, the typical extracellular signals of hippocampal neurons in spontaneous firing state were recorded as shown in Fig. 4A (Ch22 and Ch68, Bessel 4-order high-pass filter, cut-off frequency: 250 Hz). The signal baseline was less than 20 μV, and the action potential amplitude was more than 100 μV. Thus, the signal-to-noise ratio was more than 5, which proved that the neuronal potentials were effectively recorded by the MEA chip. Three-fold Sigma was chosen as the threshold to detect the spike of each channel. Waveform, positive-to-negative-peak duration, peak-to-peak value and other characteristic features were extracted to classify four types of spike as shown in Fig. 4B. Generally, the positive and negative peak intervals of interneurons are less than 500 μs, while the pyramidal neurons' intervals are more than 700 μs (Barthó et al., 2004). Therefore, the first three kinds of spikes originate from the firing of interneurons, and the last one is from pyramidal neurons.

The spike rasters and rate histograms of interneurons and pyramidal neurons firing rates (spontaneous, 10 min, 3 h, 12 h and 24 h after the treatment with AβOs) are presented in Fig. 4C. Both neurons had a short-term stress response after the treatment with AβOs. The firing rate of interneurons increased abruptly, while the firing rate of pyramidal neurons disappeared temporarily. They both gradually returned to original spontaneous state after 10 min. After 3 h, the firing rate increased significantly caused by enhanced calcium influx generated by AβOs co-localized with axonal voltage-gated calcium channels. It resulted in an abnormally high level of glutamate in the extracellular space and improved spontaneous postsynaptic activity. After that, AβOs gradually reduced the number of dendritic spines, increased synaptic protein loss, and compromised the surface expression of neurotransmitter receptors. This occurs together with a reduction of excitatory postsynaptic currents and impairment of synaptic plasticity. After 12 h, the firing rates of interneurons and pyramidal neurons decreased in varying degrees. The pyramidal neurons firing disappeared completely after 24 h while the interneurons firing still excited. The pyramidal neurons firing was more seriously affected because the pyramidal neurons are central to the pathogenesis and cognitive dysfunction of AD. They are the site of tangle formation with the mismetabolism of APP (Greene et al., 2010). The neurofibrillary tangle formation affected predominantly pyramidal neurons and many of these cells subsequently died and disappeared.

The positive and negative spike intervals of the two types of neurons at different time points are shown in Fig. 4D. The average positive and negative spike intervals of the interneurons are 479 ± 6.2 μs, while the intervals of pyramidal neurons are 691 ± 14.1 μs. The positive and negative spike intervals between the two types of neurons have no significant difference except that the pyramidal neurons firing disappears after 24 h. The firing rates and peak-to-peak values of interneurons and pyramidal neurons at different time points are shown in Fig. 4E and F, respectively. There is no significant difference between the interneurons and pyramidal neurons in spontaneous state, 10 min, 3 h and 12 h after the treatment with AβOs, while the peak-to-peak values of the interneurons reduced a little after 24 h.

3.4. Hippocampal neuronal network firing mapping

Neuronal degeneration, interruption of network connection and communication are the major pathological changes of AD brain (Vickers et al., 2000). Fig. 5 shows the multi-site signals of neuronal network recorded simultaneously by the MEA chip. The spontaneous firing state is illustrated in Fig. 5A. Half of the sixty channels recorded

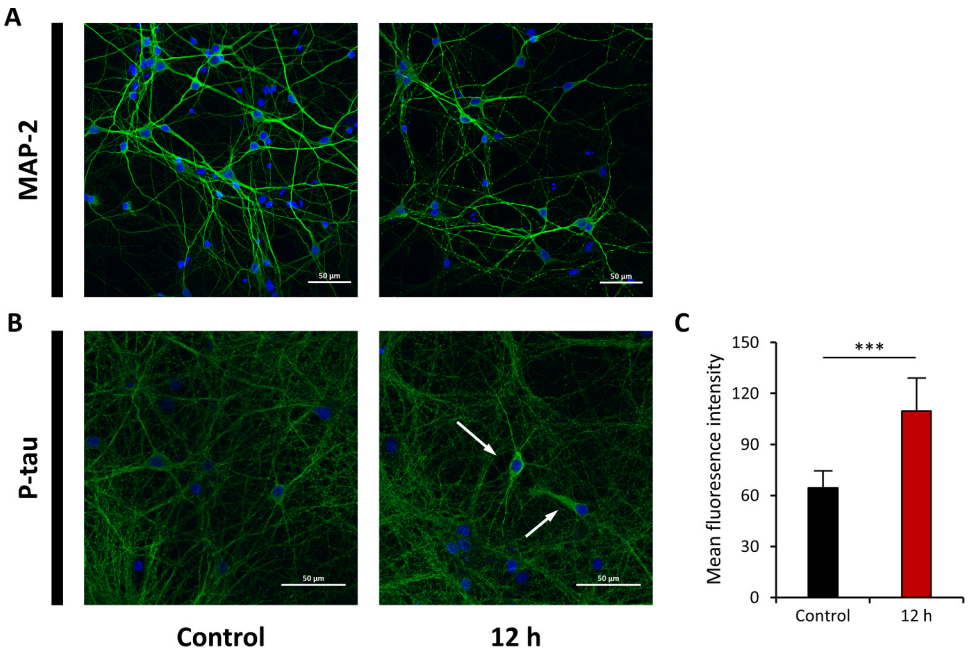

Fig. 3. Immunofluorescence of hippocampal neuron (13 d) stained with antibodies against markers MAP2 and p-Tau protein. (a) Immunofluorescence staining for MAP2 (control and treated with AβOs for 12 h). (b) Immunofluorescence staining for p-tau (control and treated with AβOs for 12 h) and neuron with tau hyperphosphorylation (white arrows). (c) Quantification of p-tau levels in control and AβOs-treated neurons. Y axis values represent mean fluorescence intensity of each p-tau band. Data are represented by the mean ± SD. Student's *t*-test was used to evaluate difference significance between 12 h *versus* control (***P < 0.001, n = 9 represent the number of single neuron in different visual fields).

baseline signals, while two channels have abnormal signals, and the other twenty-eight channels recorded effective firing signals of hippocampal neuronal network. Among them, spikes recorded in twelve channels were interneurons (orange), while spikes recorded in sixteen channels were pyramidal neurons (blue). According to the location of the electrodes and the channel distribution, the interneurons and pyramidal neurons were distributed in blocks. The extracellular electrical signals of the soma or axon dendrites of the same neurons were recorded at the similar electrodes. The signal firing of hippocampal neuronal network at 3 h after the treatment with AβOs is shown in Fig. 5B. The number of effective signal channels stays the same, and the spike firing of most channels increases under the short-term effect of AβOs-induced. The neuronal network firing at 12 h after the treatment with AβOs is shown in Fig. 5C. The signal of Ch28 and Ch38 disappeared and spike firing decreased in most channels under the long-term effect of AβOs. The AβOs-treated neuronal network after 24 h is shown in Fig. 5D. The signals among twenty-one channels disappeared, and six of the remaining channels were interneurons. The firing frequency and amplitude were significantly reduced. Only one channel of pyramidal neurons was still recorded.

3.5. Cross-correlation analysis

MEA has the virtue of simultaneous recording from multi-sites, which is favorable to explore the characteristics as well as the relationship among the multi-channel signals. The similarity as well as synchrony between channels can be depicted by cross-correlation analysis (Qingmei et al., 2011). Our neuronal network chip system investigated the synchronization and parallel relationship between neuron and neuron information. The cross-correlation analysis of the firing of similar channel neurons in four groups (interneurons: Ch12 vs Ch22, Ch62 vs Ch74; pyramidal neurons: Ch27 vs Ch28, Ch43 vs Ch47) is shown in Fig. 5E. If the cross-correlation histogram is flat and irregular, the two firing sequences are considered as independent processes. If one peak shows at zero point, the two neurons tend to fire synchronously with common input or synaptic connection between them. The cross-correlation of neurons firing recorded between Ch12 and Ch22, Ch43 and Ch47 are synchronized with refractory periods in the spontaneous firing state, which indicates that the same neuron firing was recorded. Moreover, the cross-correlation histogram between Ch62 and Ch74, Ch27 and Ch28 shows no obvious refractory period, indicating that synchronized firing of different neurons was recorded. After 3 h of the treatment with AβOs, the strong correlation among the four group channels still existed. After 12 h, except for Ch43 and Ch47, the correlation between Ch12 and Ch22, Ch62 and Ch74 was significantly weakened, and the correlation between Ch27 and Ch28 disappeared. After 24 h, all groups had no synchronization between channels, which identified that AβOs treatment caused a progressive network dysfunction. The communication between neuronal networks was interrupted and transmission of signals and nutrients was blocked.

3.6. Electrical stimulation on hippocampal neuronal network

MEA micro-stimulation is currently being considered for the elaboration of neural prosthesis for the rehabilitation of the injured central nervous system (Humayun et al., 2003; Mccreery et al., 2007; Saigal et al., 2004). The stimulation frequency that was set up at 40 Hz according to the driving 40 Hz gamma oscillations may induce an overall neuroprotective response that recruits both neurons and microglia (Iaccarino et al., 2017). After 12 h of the treatment with AβOs, electrical stimulation signals with different amplitudes of 40 Hz (stimulation duration: 10 s) were released at one working electrode. Changes of neuronal firing signals in the nearby effective channels were recorded as shown in Fig. 6. When the peak-to-peak value of stimulation was 187 mV (Fig. 6A) or 137 mV (Fig. 6B), the neurons excitatory response was observed after electrical stimulation. However, the stimulation with 67 mV (Fig. 6C) inhibits neuronal firing. The firing rate increased significantly or disappeared within 30 s, and then gradually returned to the spontaneous frequency in the following 30 s. When the frequency of stimulation decreased (4 Hz), electrical stimulation had no effect on the firing of hippocampal neurons, and the firing rate had no significant difference between before and after stimulation (Fig. 6D). The effect of electrical stimulation on the firing of hippocampal neuronal network is preliminarily presented in this paper, which provides the possibility for evaluation of the therapeutic effect of electrical stimulation.

4. Conclusions

In this paper, a pathological model of AD in vitro based on the hippocampal neuronal network chip was established for multi-site and long-term monitoring of bioelectrical activity changes in neurodegenerative networks. The dynamics activities of interneurons and

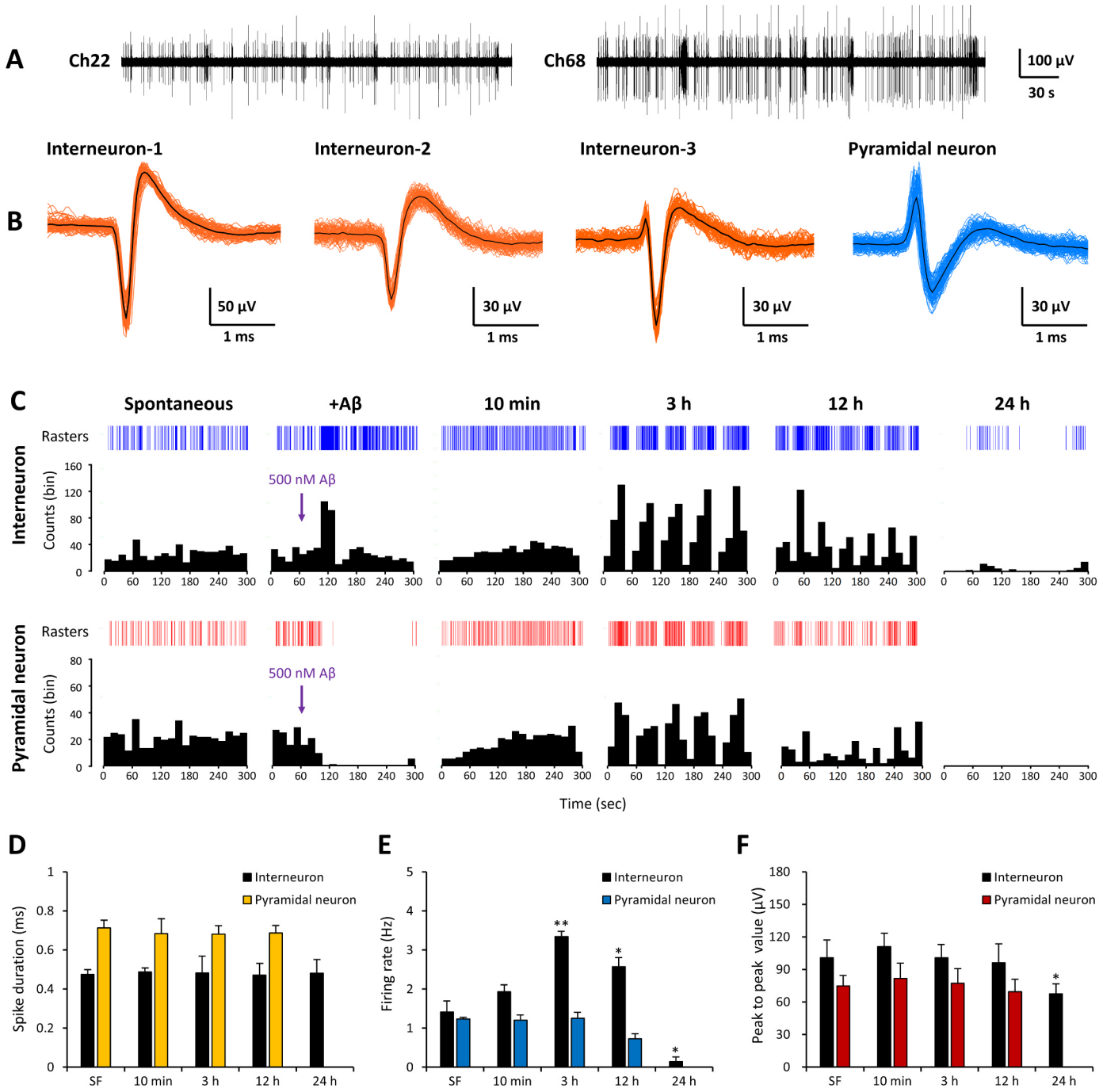

Fig. 4. Spike firing from hippocampal neuronal network recorded via the MEA chip and system for analysis. (a) The typical extracellular signals of hippocampal neurons in spontaneous firing state (e.g. Ch22 and Ch68). (b) The extracted waveform, positive-to-negative-peak duration, peak-to-peak value and other characteristic features to classify four types of spike. (c) The spike rasters and rate histograms of interneurons and pyramidal neurons firing (spontaneous, 10 min, 3 h, 12 h and 24 h after the treatment with AβOs). (d) The positive and negative spike intervals, (e) the firing rates and (f) peak-to-peak values of interneurons and pyramidal neurons at different time points. Data are represented by the mean ± SD. Student's *t*-test was used to evaluate difference significance between 10 min, 3 h, 12 h and 24 h versus spontaneous (*P < 0.05, **P < 0.01, n = 7 represent the number of valid recording electrodes).

pyramidal neurons induced by AβOs within 24 h were recorded. The excitability was enhanced in the early stage, while it gradually reduced after 12 h, and the pyramidal neurons firing eventually disappeared. AβOs treatment caused a progressive network dysfunction, and the spatial firing patterns map and cross-correlation between channels were performed to validate the degeneration of neuronal network connectivity. In addition, the effect of electrical stimulation on the firing of hippocampal neuronal network was preliminarily explored. This neuronal network chip enables the detection of the AβOs toxicity responses, the identification of connectivity and interactions within neuronal networks, and the characterization of the effect of potential therapeutics, which can be a novel technique in the research of AD pathological model *in vitro*.

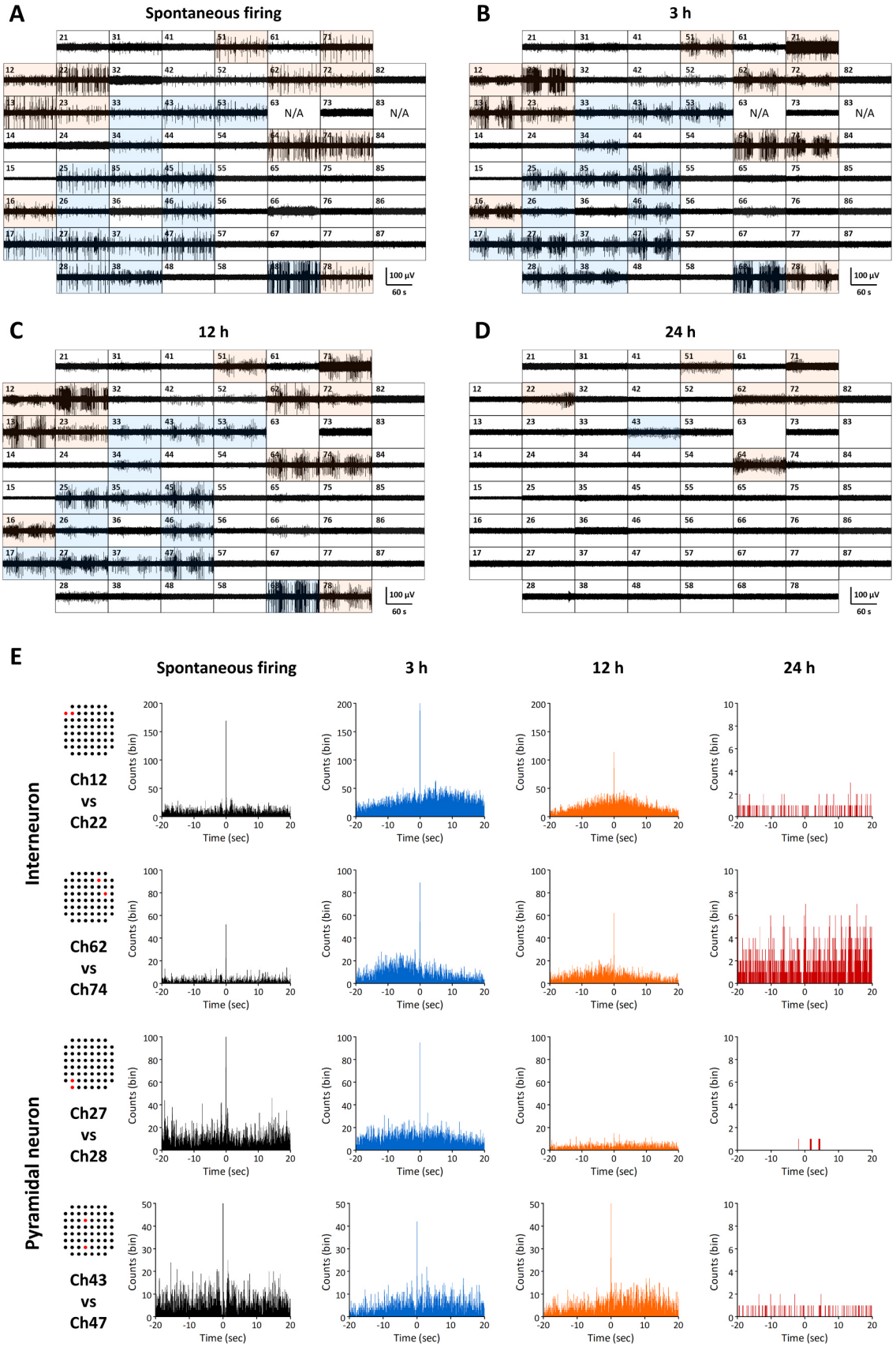

Fig. 5. The multi-site signals of hippocampal neuronal network recorded simultaneously by MEA chip. (a) Spontaneous firing. (b) 3 h after the treatment with AβOs. (c) 12 h after the treatment with of AβOs. (d) 24 h after the treatment with AβOs. (e) The cross-correlation analysis of the firing of similar channel neurons in four groups (interneurons: Ch12 vs Ch22, Ch62 vs Ch74; pyramidal neurons: Ch27 vs Ch28, Ch43 vs Ch47).

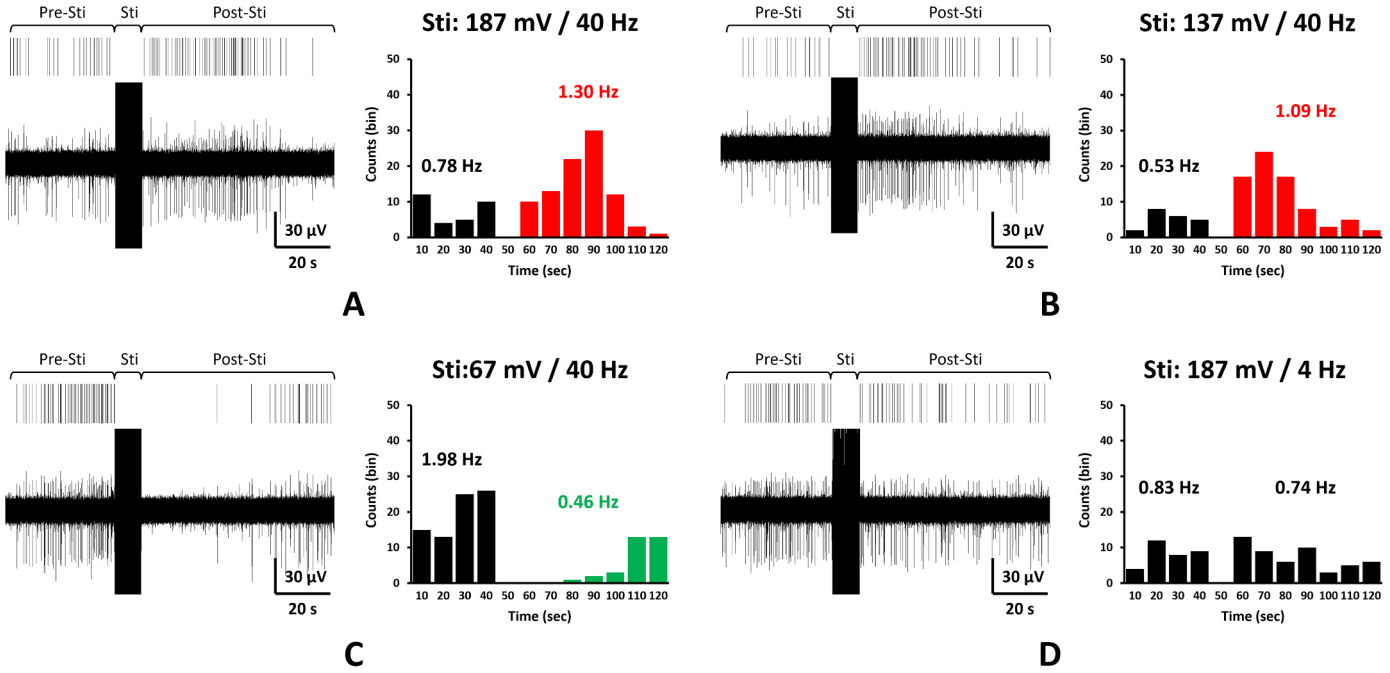

Fig. 6. The electrical stimulation with different amplitudes and frequency on hippocampal neuronal network. (a) 187 mV/40 Hz. (b) 137 mV/40 Hz. (c) 67 mV/40 Hz. (d) 187 mV/4 Hz.

CRediT authorship contribution statement

Fan Gao: Conceptualization, Methodology, Data curation, Software, Formal analysis, Validation, Writing - original draft, Writing - review & editing. **Keqiang Gao:** Conceptualization, Methodology, Data curation, Software, Formal analysis, Validation, Writing - original draft, Writing - review & editing. **Chuanjiang He:** Conceptualization, Methodology, Formal analysis, Validation, Writing - original draft, Writing - review & editing. **Mengxue Liu:** Conceptualization, Methodology, Formal analysis, Validation, Writing - original draft, Writing - review & editing. **Hao Wan:** Formal analysis, Validation, Writing - review & editing. **Ping Wang:** Conceptualization, Methodology, Formal analysis, Validation, Writing - original draft, Writing - review & editing.

Acknowledgements

This work was supported by Development Project of National Major Scientific Research Instrument (No. 31627801), Science and Technology Department of Zhejiang Province (No. 2019C03066), National Natural Science Foundation of China (No. 81811530116). Also it is grateful to Miss S. S. Liu for help in confocal scanning microscope.

Declaration of interests

None.

Appendix A. Supporting information

Supplementary data associated with this article can be found in the online version at doi:10.1016/j.bios.2019.03.025.

References

Alessandro, M., Mauro, G., Mariateresa, T., Thierry, N., Kilian, I., Sergio, M., Luca, B., 2010. Front Neuroeng. 3 (4), 1–12.
Amin, H., Nieus, T., Lonardoni, D., Maccione, A., Berdondini, L., 2017. Sci. Rep. 7 (1), 2460–2473.
Andermann, M.L., Kerlin, A.M., Reid, R.C., 2010. Front Cell Neurosci. 4 (1), 1–16.
April, J., Mcbain, C.J., André, F., 2015. J. Physiol. 592 (19), 4187–4199.
Barthó, P., Hirase, H., Monconduit, L., Zugaro, M., Harris, K.D., Buzsáki, G., 2004. J. Neurophysiol. 92 (1), 600–608.
Berdondini, L., Overstolz, T., De Rooij, N.F., Koudelka-Hep, M., Wany, M., Seitz, P., 2001. IEEE International Conference on Electronics.
Bomfim, T.R., Forny-Germano, L., Sathler, L.B., Brito-Moreira, J., Houzel, J.C., Decker, H., Silverman, M.A., Kazi, H., Melo, H.M., McClean, P.L., Holscher, C., Arnold, S.E., Talbot, K., Klein, W.L., Munoz, D.P., Ferreira, S.T., De Felice, F.G., 2012. J. Clin. Investig. 122 (4), 1339–1353.
Cai, X., Kallarackal, A.J., Kvarta, M.D., Goluskin, S., Gaylor, K., Bailey, A.M., Lee, H.K., Huganir, R.L., Thompson, S.M., 2013. Nat. Neurosci. 16 (4), 464–U135.
Charkhkar, H., Meyyappan, S., Matveeva, E., Moll, J.R., Mchail, D.G., Peixoto, N., Cliff, R.O., Pancrazio, J.J., 2015. Brain Res. 1629, 1–9.
Cottance, M., Nazeer, S., Rousseau, L., Lissorgues, G., Joucla, S., Yvert, B., Lewis, N., Bornat, Y., Renaud, S., 2013. New Circuits & Systems Conference.
De Felice, F.G., Velasco, P.T., Lambert, M.P., Viola, K., Fernandez, S.J., Ferreira, S.T., Klein, W.L., 2007. J. Biol. Chem. 282 (15), 11590–11601.
Decker, H., Lo, K.Y., Unger, S.M., Ferreira, S.T., Silverman, M.A., 2010. J. Neurosci. 30 (27), 9166–9171.
Eversmann, B., Jenkner, M., Hofmann, F., Paulus, C., Brederlow, R., Holzapfl, B., Fromherz, P., Merz, M., Brenner, M., Schreiter, M., 2003. IEEE J. Solid-St Circ. 38 (12), 2306–2317.
Franks, W., Heer, F., Mckay, I., Taschini, S., Sunier, R., Hagleitner, C., Hierlemann, A., Baltes, H., 2003. International Conference on Transducers, Solid-state Sensors, Actuators & Microsystems.
Gan, K.J., Silverman, M.A., 2015. Mol. Biol. Cell. 26 (6), 1058–1071.
Geng, D., Kang, L., Su, Y., Jia, J., Ma, J., Li, S., Du, J., Cui, H., 2013. Neurochem Int. 63 (4), 283–290.
Greene, J.R., Radenahmad, N., Wilcock, G.K., Neal, J.W., Pearson, R.C., 2010. Neuropathol. Appl. Neurobiol. 27 (5), 339–342.
Hu, L., Wang, Q., Qin, Z., Su, K., Huang, L., Hu, N., Wang, P., 2015. Biosens. Bioelectron. 66, 572–578.
Humayun, M.S., Weiland, J.D., Fujii, G.Y., Greenberg, R., Williamson, R., Little, J., Mech, B., Cimmarusti, V., Boemel, G.V., Dagnelie, G.J.V.R., 2003. Vision Res. 43 (24), 2573–2581.
Hyman, B.T., Phelps, C.H., Beach, T.G., Bigio, E.H., Cairns, N.J., Carrillo, M.C., Dickson, D.W., Duyckaerts, C., Frosch, M.P., Masliah, E., Mirra, S.S., Nelson, P.T., Schneider, J.A., Thal, D.R., Thies, B., Trojanowski, J.Q., Vinters, H.V., Montine, T.J., 2012. Alzheimers Dement. 8 (1), 1–13.
Iaccarino, H.F., Singer, A.C., Martorell, A.J., Rudenko, A., Gao, F., Gillingham, T.Z., Mathys, H., Seo, J., Kritskiy, O., Abdurrob, F., 2017. Nature 540 (7632), 230–235.
Kanaan, N.M., Morfini, G., Pigino, G., Lapointe, N.E., Andreadis, A., Song, Y., Leitman, E., Binder, L.I., Brady, S.T., 2012. Neurobiol. Aging 33 (4), 826.e815–826.e830.
Keefer, E.W., Norton, S.J., Boyle, N.A.J., Talesa, V., Gross, G.W., 2001. Neurotoxicology 22 (1), 3–12.
Lambert, M.P., Barlow, A.K., Chromy, B.A., Edwards, C., Freed, R., Liosatos, M., Morgan, T.E., Rozovsky, I., Trommer, B., Viola, K.L., 1998. P Natl. Acad. Sci. USA 95 (11), 6448–6453.
Li, C., Götz, J., 2017. Embo J. 36 (21), 3120–3138.
Lu, K.T., Gean, P.W., 1998. Neuroscience 86 (3), 729–737.
Mccreery, D., Lossinsky, A., Pikov, V., 2007. IEEE T Bio-Med Eng. 54 (1), 1042–1052.
Mcinnes, J., Wierda, K., Snellinx, A., Bounti, L., Wang, Y.C., Stancu, I.C., Apóstolo, N.,

Gevaert, K., Dewachter, I., Spires-Jones, T.L., 2018. Neuron 97 (4), 823–835.
Morris, M., Maeda, S., Vossel, K., Mucke, L., 2011. Neuron 70 (3), 410–426.
Novellino, A., Scelfo, B., Palosaari, T., Price, A., Sobanski, T., Shafer, T.J., Johnstone, A.F., Gross, G.W., Gramowski, A., Schroeder, O., Jugelt, K., Chiappalone, M., Benfenati, F., Martinoia, S., Tedesco, M.T., Defranchi, E., D'Angelo, P., Whelan, M., 2011. Front Neuroeng. 4, 1–14.
Qingmei, C., Lidan, X., Qingjun, L., Shucai, L., Yifei, Y., Qi, D., Ping, W., 2011. Biosens. Bioelectron. 26 (7), 3313–3319.
Robinette, B.L., Harrill, J.A., Mundy, W.R., Shafer, T.J., 2011. Front Neuroeng. 4 (4), 1–9.
Saigal, R., Renzi, C., Mushahwar, V.K., 2004. IEEE Trans Neural Syst. Rehab. 12 (4), 430–440.
Scheefhals, N., MacGillavry, H.D., 2018. Mol. Cell Neurosci. 91, 82–94.
Se Hoon, C., Young Hye, K., Matthias, H., Christopher, S., Seungkyu, L., Carla, D.A., Hechao, C., Basavaraj, H., Caroline, A., Julien, M., 2011. Nature 515 (7526), 274–278.
Sheng, M., Sabatini, B.L., Sudhof, T.C., 2012. Cold Spring Harb. Perspect. Biol. 4 (5), 747–749.
Sosa, L.J., Caceres, A., Dupraz, S., Oksdath, M., Quiroga, S., Lorenzo, A., 2017. J. Neurochem. 143 (1), 11–29.
Stern, J.L., Lessard, D.V., Hoeprich, G.J., Morfini, G.A., Berger, C.L., 2017. Mol. Biol. Cell. 28 (8), 1079–1087.
Stett, A., Egert, U., Guenther, E., Hofmann, F., Meyer, T., Nisch, W., Haemmerle, H., 2003. Anal. Bioanal. Chem. 377 (3), 486–495.
Tang, Y., Ye, M., Du, Y., Qiu, X., Lv, X., Yang, W., Luo, J., 2015. Neuroscience 304, 109–121.
Tu, S., Okamoto, S.I., Lipton, S.A., Xu, H.J.M.N., 2014. Mol. Neurodegener. 9 (1), 48–60.
Vickers, J.C., Dickson, T.C., Adlard, P.A., Saunders, H.L., King, C.E., Mccormack, G., 2000. Prog. Neurobiol. 60 (2), 139–165.
Yang, Q., Ke, Y., Luo, J., Tang, Y., 2016. J. Neurosci. Methods 277, 38–45 (Complete).